Marine and Petroleum Geology 127 (2021) 104957

Contents lists available at ScienceDirect

Marine and Petroleum Geology

journal homepage: www.elsevier.com/locate/marpetgeo

Interactions between deep formation fluid and gas hydrate dynamics inferred from pore fluid geochemistry at active pockmarks of the Vestnesa Ridge, west Svalbard margin

W.-L. Hong [a,b,c,1,*], T. Pape [d], C. Schmidt [e], H. Yao [b], K. Wallmann [e], A. Plaza-Faverola [b], J.W. B. Rae [f], A. Lepland [a,b], S. Bünz [b], G. Bohrmann [d]

[a] Geological Survey of Norway (NGU), Trondheim, Norway
[b] Centre for Arctic Gas Hydrate, Environment and Climate (CAGE), Department of Geosciences, UiT The Arctic University of Norway, N-9037, Tromsø, Norway
[c] Department of Geological Sciences, Stockholm University, Stockholm, Sweden
[d] MARUM–Centre for Marine Environmental Sciences and Faculty of Geosciences, University of Bremen, Bremen, Germany
[e] GEOMAR Helmholtz Centre for Ocean Research, Kiel, Germany
[f] School of Earth and Environmental Sciences, University of St. Andrews, St. Andrews, UK

ARTICLE INFO

Keywords:
Pockmark
Gas hydrate
MeBo drilling
Isotope geochemistry

ABSTRACT

Seafloor seepage sites along the Vestnesa Ridge off west-Svalbard have been, for decades, a natural laboratory for the studies of fluid flow and gas hydrate dynamics along passive continental margins. The lack of ground truth evidence for fluid composition and gas hydrate abundance deep in the sediment sequence however prohibits us from further assessing the current model of pockmark evolution from the region. A MARUM-MeBo 70 drilling cruise in 2016 aims to advance our understanding of the system by recovering sediments tens of meters below seafloor from two active pockmarks along Vestnesa Ridge. We report pore fluid composition data focusing on dissolved chloride, stable isotopes of water ($\delta^{18}O$ and δD), and the isotopic composition of dissolved boron ($\delta^{11}B$). From one of the seepage sites, we detect a saline formation water with two layers where gas hydrates were recovered. This saline formation pore fluid is characterized by elevated chloride concentrations (up to 616 mM), high B/Cl ratios (9×10^{-4} mol/mol), high $\delta^{18}O$ and δD isotopic signatures (+0.6‰ and +3.8‰, respectively) and low $\delta^{11}B$ signatures (+35.0‰), which collectively hint to a high temperature modification at great depths. Based on the dissolved chloride concentration profiles, we estimated up to 47% of pore space occupied by gas hydrate in the sediments shallower than 11.5 mbsf. The observation of bubble fabric in the recovered gas hydrates suggests formation during past periods of intensive gaseous methane seepage. The presence of these gas hydrates without associated positive anomalies in dissolved chloride concentrations however suggests that the decomposition of gas hydrate is as fast as its formation. Such a state of gas hydrates can be attributed to a relatively low methane supply transported by the saline formation water at present. Our findings based on pore fluid composition corroborate previous inferences along Vestnesa Ridge that fluids sustaining seepage have migrated from great depths and that the variable gaseous and aqueous phases through the gas hydrate stability zone control the distributions of authigenic carbonates and gas hydrates.

1. Introduction

Pockmarks are seafloor manifestations of sub-surface fluid discharge across the sediment-water interface (Hovland et al., 2002; Hovland and Svensen 2006). The presence of pockmarks has been reported from a large water depth range comprising continental shelf (e.g., Hovland et al., 2002) to deep sea regions (e.g., Ondréas et al., 2005; Sahling et al., 2008; Marcon et al., 2014; Sultan et al., 2014). Pockmarks in association with deep water gas hydrate systems have also been long recognized along the Vestnesa Ridge off the west Svalbard margin (Vogt et al. 1994, 1999). For decades, the Vestnesa Ridge pockmarks are natural laboratories for studying methane seepage along the passive continental

* Corresponding author. Geological Survey of Norway (NGU), Trondheim, Norway.
E-mail address: wei-li.hong@geo.su.se (W.-L. Hong).
[1] Current address: Department of Geological Sciences, Stockholm University.

https://doi.org/10.1016/j.marpetgeo.2021.104957
Received 22 September 2020; Received in revised form 12 October 2020; Accepted 2 February 2021
Available online 11 February 2021

margin. There are pockmarks along the ridge with the active ones, as inferred from the seepage activities by sonar data, located at the eastern Vestnesa Ridge segment (e.g., Smith et al., 2014; Bünz et al., 2012). These pockmarks have been studied for their sub-surface fluid plumbing systems (Bünz et al., 2012, Goswami et al., 2017, Knies et al., 2018, Singhroha et al., 2019, 2019), seepage periodicity and its link to tectonic stress and glacial history over geological time (Plaza-Faverola et al., 2015; Plaza-Faverola and Keiding 2019; Himmler et al., 2019), controls of gas hydrate stability zone dynamics (Plaza-Faverola et al., 2017), gas flux in the water column (Smith et al., 2014), as well as sources of light hydrocarbons and the biogeochemical consequence of fluid flow through fractures (Hong et al., 2016; Yao et al., 2019; Pape et al., 2020). All the active pockmarks along Vestnesa Ridge are connected to chimney-like conduits characterized by brecciation/fracturing of the sediment that result in scattering of the seismic signal (e.g., Petersen et al., 2010; Plaza-Faverola et al., 2015; Waage et al., 2019). These fault-associated conduits were regulated by tectonic stress and glacial dynamics with more persistent seepage activities since the Pleistocene (Plaza-Faverola et al., 2015; Knies et al., 2018; Plaza-Faverola and Keiding 2019). However, it is not clear how the composition of this long-lasting fluid system evolves during the history of these pockmarks as ground truth observations beyond a few meters subsurface are not yet available along the ridge. Specifically, substantial knowledge gaps exist in the geochemical composition of fluids as well as the interplay between pockmark evolution, near-seafloor gas hydrate dynamics and fluid migration at a meter-scale. Such a lack of information hinders the evaluation of the present model about pockmark evolution from Vestnesa Ridge. During the 2016 MARUM-MeBo drilling campaign (MeBo stands for Meeres-boden-Bohrgerät for seafloor drill rig in German), we obtained pore fluid samples from as deep as 16 m below seafloor (mbsf) from the Lunde and Lomvi pockmarks (Bohrmann et al., 2017), two of the active pockmarks in terms of seafloor gas emissions along Vestnesa Ridge (Bünz et al., 2012). The results obtained from this unique set of samples provide the ground truths for fluid sources and gas hydrate dynamics in shallow depths.

For such purposes, we report pore fluid composition (concentrations of chloride and boron) and isotopic ratios ($\delta^{18}O$–H_2O, δD-H_2O, and $\delta^{11}B$). Dissolved chloride is a conservative tracer whose concentration is unaffected by biogeochemical activities. Downcore chloride concentration profiles have been widely used to infer the in-situ production and consumption of water (such as due to gas hydrate dissociation and formation) as well as physical mixing of water from different sources (e.g., Kastner et al., 1991; Torres et al., 2011; Kim et al., 2013; Kim et al., 2016; Wallmann et al., 2018; Hong et al., 2019). Positive chloride concentration anomalies could occur when gas hydrate is actively forming and expelling chloride at a rate much higher than chloride diffusion, which results in the accumulation of chloride in the pore fluid (Ussler and Paull 2001). Such anomalies have been successfully applied to infer formation conditions and quantify the rates of gas hydrate formation in numerous studies (e.g., Ussler and Paull 2001; Haeckel et al., 2004; Milkov et al., 2004; Torres et al. 2004, 2011; Tomaru et al., 2006; Peszynska et al., 2016; Hong and Peszynska 2018).

To further differentiate the various processes in the pore fluid, $\delta^{18}O$–H_2O and δD-H_2O (hereafter as $\delta^{18}O$ and δD throughout the text) could serve as additional constraints (e.g., Kastner et al., 1991; Martin et al., 1996; Hong et al., 2019; Chen et al., 2020). Different diagenetic processes, such as authigenic clay transformation, ion filtration as well as gas hydrate formation and decomposition, result in variable degrees of fractionation on $\delta^{18}O$ and δD (Kastner et al., 1991; Maekawa et al., 1995). Dissolved boron, a minor constituent in the pore fluid but abundant in various silicate minerals (see the review by Marschall 2018 and references therein), could be used to detect the modification of fluids by silicate minerals under elevated temperatures. The diagenetic reactions that involve silicate minerals (such as clays) release abundant dissolved boron with low $\delta^{11}B$ values due to the large isotopic fractionation associated with boron desorption under medium to high temperatures (Palmer et al., 1987; Spivack et al., 1987; You et al., 1995a, b; James and Palmer 2000). Repeated observations of these distinct $\delta^{11}B$ signatures in pore fluids, and later confirmed by laboratory experiments, have proven the applicability of the boron proxy to evaluate the origin of fluids generated at greater depths (You et al., 1995a, b, 1996; Deyhle and Kopf 2001; Kopf and Deyhle 2002; Hüpers et al., 2016).

2. Materials and methods

2.1. Drilling/coring sites during cruise MSM57-1/-2

The sediment cores studied herein (Table 1) were collected at a water depth of ca. 1200 m during the cruise MSM57-1/-2 onboard 'RV MARIA S. MERIAN' with the seafloor drill rig MARUM-MeBo70 (Freudenthal and Wefer 2013). Coring positions were determined by high resolution bathymetry data collected during a cruise no.1606 onboard R/V G.O. Sars a few months before the MSM57 cruise (Fig. 1b). We combined the results from gravity cores taken close to MeBo drill sites to obtain a better coverage in the uppermost few meters of the sediments (Table 1). The three locations investigated from the Lunde pockmark include a non-seepage site from the central depression of the pockmark (GeoB21601-1, GeoB21605-1, and GeoB21610-1) and two sites with high methane fluxes (SW seepage site: GeoB21621-1 & GeoB21637-1 and SE seepage site: GeoB21619-1) (Fig. 1b). As a comparison to the Lunde pockmark, we also report results from two gravity cores recovered from the seepage area of the Lomvi pockmark (GeoB21623-1 & GeoB21624-1). In addition, a reference site with low methane flux (GeoB21606-1 & GeoB21613-1) that is outside any pockmark footprint is included (Fig. 1a). Gas hydrates were only recovered from the seepage sites of both pockmarks (Fig. 1a and 1b).

2.2. Pore water sampling and analyses

The procedures for sediment core handling were detailed in Bohrmann et al. (2017). Briefly, sectioning of the sediment cores was done at an ambient temperature of ~10 °C. Before splitting the core into two halves, the surfaces of the core liners were scanned with infrared radiation (IR) camera (see Pape et al., 2020) to detect negative thermal anomalies that are associated with the endothermic gas hydrate dissociation (Tréhu et al., 2004). We sampled 2–3 cm sections and 8–10 cm sections from the working halves of the gravity cores and the MeBo cores, respectively, for pore water extraction by using the GEOMAR argon-gas squeezers. In average, it took 30–45 min to squeeze 5–10 ml of pore water. Squeezing was performed in a +4 °C refrigerated room. Gas pressure was monitored and never exceeded 5 bars during the squeezing. Water samples from hydrate-bearing sediments were also

Table 1
Specifics of sediment cores investigated in this study. Refer to Bohrmann et al. (2017) and Pape et al. (2020) for exact positions. Additional data on the sediment cores are made available through the PANGAEA data publisher (https://www.pangaea.de/).

Site	Core code [GeoBXXXXX-X]	Tool-site #	Cored/Drilled Depth [mbsf]
Reference site	21606–1	GC-3	5.84
	21613–1	MeBo-126	62.50
Lunde pockmark	21601–1	GC-1	5.77
non-seepage site	21605–1	GC-2	7.65
	21610–1	MeBo-125	22.80
Lunde pockmark	21621–1	MeBo-128	7.75
SW seepage site	21637–1	MeBo-138	23.95
Lunde pockmark	21619–1	GC-9	4.78
SE seepage site			
Lomvi pockmark	21623–1	GC-11	1.55
	21624–1	GC-12	2.62

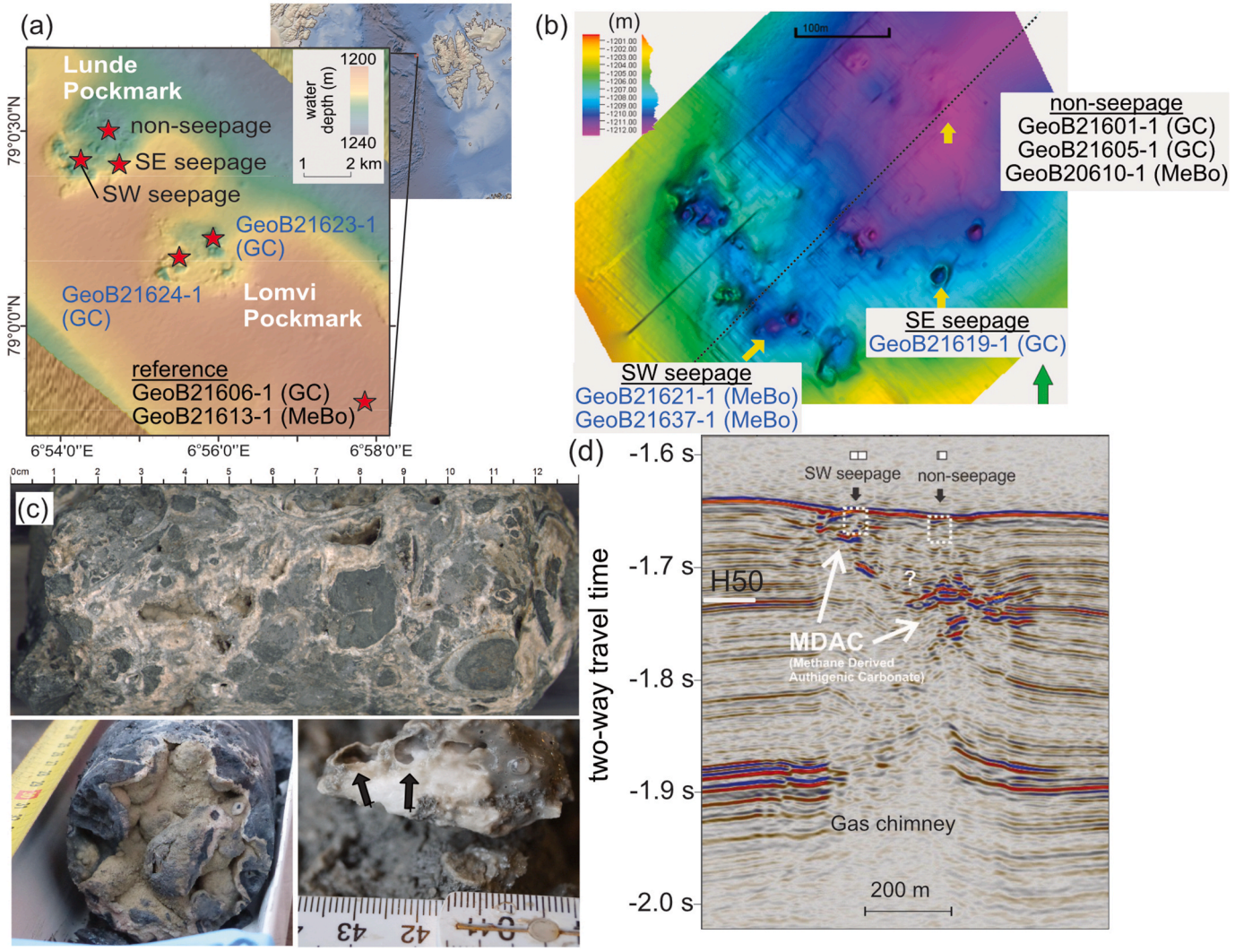

Fig. 1. Location maps, seismic data, and core photos from the investigated pockmarks along Vestnesa Ridge. (a) An overview map for Vestnesa Ridge with detailed bathymetry from the Lunde and Lomvi pockmarks (see Table 1 for core details). The locations of the three study sites from Lunde pockmark (non-seepage, SW seepage, and SE seepage) and the reference site are indicated. Cores with recovery of gas hydrate are labeled in blue. GC: gravity core. (b) High resolution bathymetry of the Lunde pockmark (Himmler et al., 2019) with a NE-SW-trending seismic line across the pockmark shown in (d). Cores with recovery of gas hydrate were labeled in blue. MeBo: cores obtained by a MeBo seafloor drill rig. (c) Photographs of carbonate-cemented sediments and gas hydrates with bubble fabric (black arrows) recovered from the Lunde SW and SE seepage sites. (d) A seismic profile showing the sub-surface structure of the Lunde pockmark. The dashed white boxes showing roughly the penetration of the drilling from the Lunde non-seepage and SW seepage sites. The high reflectance in the seismic data was interpreted as buried carbonate-cemented sediment strata (Plaza-Faverola et al., 2015) which is confirmed by the presence of seep carbonate formations (or MDAC, methane-derived authigenic carbonate, in the figure) in the drilled cores that are the results of past methane seepage activities (Himmler et al., 2019). (For interpretation of the references to colour in this figure legend, the reader is referred to the Web version of this article.)

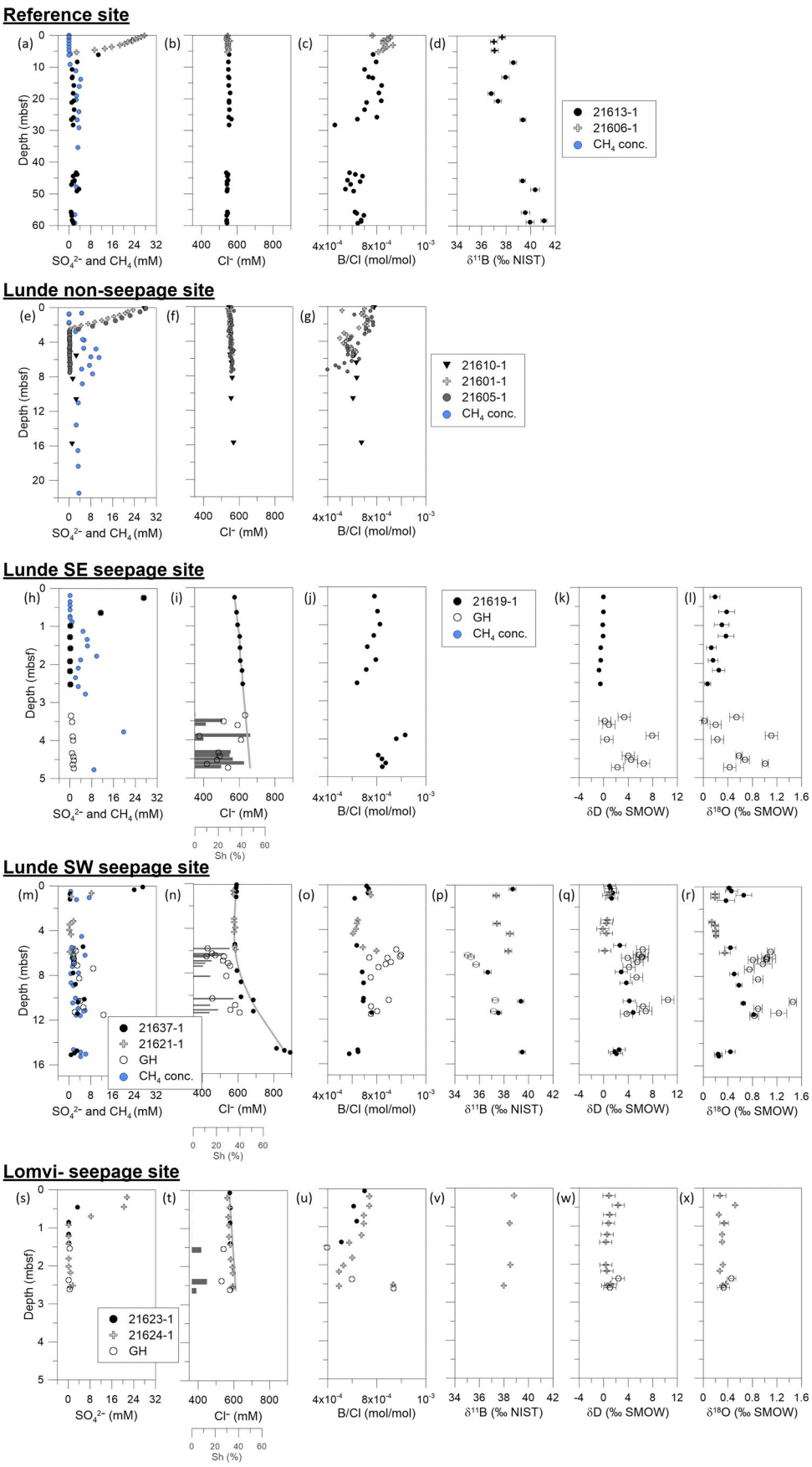

Fig. 2. Pore fluid profiles of sulfate, methane, chloride ([Cl]), $\delta^{18}O$, δD, B/Cl ratio, and $\delta^{11}B$ in MeBo and gravity cores from the investigated sites in the Lunde and Lomvi pockmarks. "GH" stands for the pore fluid samples collected from the sediment sections containing gas hydrate. The abundance of gas hydrate (horizontal dark grey bars in subplots (i), (n), and (t); in % of pore space) was estimated from the differences between $[Cl]_{obs}$ (empty symbols) and $[Cl]_{fit}$ (grey solid lines) with the values reported in Table 2. The gaps in the geochemical profiles are due to poor recovery of sediments within those intervals. Note the different depth scales for the various sites.

collected. After gas hydrates completely dissociated, as indicated by the dissipating temperature anomalies, samples were collected with acid-washed rhizons and syringes (Seeberg-Elverfeldt et al., 2005) and treated identical to other pore water samples.

Additional water samples from dissociated gas hydrates (referred to as gas hydrate samples in the text) were analyzed for their composition and boron isotopic signatures. Three gravity cores were dedicated to recover intact gas hydrate. The gas hydrate samples were preserved within liquid nitrogen for storage at MARUM. Centimeter-sized gas hydrate subsamples were later left to dissociate at room temperature to obtain water samples from gas hydrate for analyses of cation concentrations and stable boron isotopic signatures. The hydrate-bound water was filtered with 0.2 μm disposable in-line syringe filters and preserved with acid-washed vials.

After extraction, pore water was divided into sub-samples for further analysis. Downcore methane and sulfate concentrations were reported by Pape et al. (2020) and are presented in Fig. 2. Shipboard analyses of dissolved chloride concentrations ([Cl]) were conducted through titration with silver nitrate as documented in Bohrmann et al. (2017). For the analyses of $\delta^{18}O$ and δD, pore water sub-samples were filled into 2 ml glass vials without headspace. Sub-samples for cations were acidified with 10 μl of concentrated reagent grade nitric acid. Separated acid-washed 1.5 ml Eppendorf vials were used for the analyses of $\delta^{11}B$ in the pore fluid. No nitric acid was added to these sub-samples. $\delta^{18}O$ and δD signatures were determined with a Delta plus XP isotope ratio mass spectrometer (Thermo Fisher Scientific) as detailed in Wallmann et al. (2018). These values are reported against the Vienna Standard Mean Ocean Water (V-SMOW) standard. For analysis of $\delta^{11}B$ in pore water, 10 μl of non-acidified samples was put through boron-specific anionic exchange resin Amberlite IRA 743 (Kiss 1988; Yoshimura et al., 1998) to isolate 2–10 ng of boron, following the protocol described by Foster (2008). Analyses of the isotopic ratios were performed with a Neptune multicollector inductively coupled plasma-mass spectrometer (MC-ICPMS) at the St. Andrews Isotope Geochemistry (STAiG) Laboratory of the University of St. Andrews following methods detailed previously (Rae et al. 2011, 2018; Foster et al., 2013) with long-term reproducibility of 0.2‰ (2σ). Values are reported against the NIST 951 standard.

2.3. Quantification of gas hydrate abundance from pore water chloride concentration profiles

During core recovery, dissociation of gas hydrate releases fresh water into the ambient pore space. This process results in lower [Cl] when comparing to the background [Cl] within the hydrate-bearing sediments (Matsumoto 2000; Ussler and Paull 2001; Hesse 2003; Torres et al., 2004; Tomaru et al., 2006; Kim et al., 2013). Through calculating the difference, we can estimate the gas hydrate saturation (S_h in Fig. 2i, 2n and 2t and Table 2). Defining the background profile of [Cl] is critical as the water samples containing or adjacent to gas hydrate may be affected by gas hydrate dissociation. We used the [Cl] from sediment samples without any sign of hydrate presence (e.g., no thermal anomaly and visual observation) to establish the background [Cl] profiles. Such an exercise was applied to the seepage sites in the Lomvi and Lunde pockmarks (Table 2 and grey lines in Fig. 2i, 2n. and 2t). For the three gravity cores with less than 5-m of recovery (GeoB21619-1 from the Lunde SE seepage site; GeoB21623-1 and GeoB21624-1 from the Lomvi pockmark), we fit the downcore [Cl] with linear regressions and extrapolated to the depth range where gas hydrates were recovered. We fit the [Cl] from hydrate-free samples of the Lunde SW seepage site with a 4th order polynomial regression to interpolate the background [Cl] for the two hydrate-bearing intervals. The values of S_h from these cores at various depths were calculated according to:

$$S_h(\%\ pore\ space) = \frac{\beta \times \left([Cl]_{obs} - [Cl]_{fit}\right)}{[Cl]_{fit} + \beta \times \left([Cl]_{obs} - [Cl]_{fit}\right)} \times 100$$

where $[Cl]_{fit}$ is the interpolated or extrapolated chloride concentrations while $[Cl]_{obs}$ is the observed chloride concentrations (Table 2). Factor β (1.257) is a dimensionless constant that accounts for the density change from gas hydrate to water during hydrate dissociation (Ussler and Paull, 2001). It is important to note that the S_h calculated with [Cl] is a first order estimation of gas hydrate abundance. From Vestnesa Ridge, it is anticipated that gas hydrates also form in fractures, which are not accounted for here.

3. Results

3.1. Downcore distribution of gas hydrates from the seepage sites in the Lunde and Lomvi pockmarks

The hydrate-bearing intervals for all the sediment cores investigated were determined by shipboard visual inspection, thermal anomalies with IR measurements, and later confirmed by the freshening observed from pore fluid composition (i.e. lower [Cl] as compared to seawater). Much shallower gas hydrate occurrences were documented from the Lunde SW seepage site by Pape et al. (2020) with a depth of 0.45 mbsf reported for the gravity core GeoB21609-1. This core is however not investigated for pore fluid geochemistry. For the two MeBo cores recovered from the Lunde SW seepage site, gas hydrates were observed exclusively from two depth intervals: 5.80 to 8.28 mbsf and 10.29 to 11.54 mbsf (Fig. 2n). Gas hydrates were sampled below 3.30 mbsf from the gravity core in the Lunde SE seepage site (Fig. 2i). Three thin layers of gas hydrates between 1.54 mbsf and 2.62 mbsf were recovered by two gravity cores from the Lomvi pockmark (Fig. 2t). Gas hydrate saturations calculated from these cores range from <1% to 47% of the pore space (Table 2).

Table 2
Estimation of gas hydrate saturation (S_h in % pore space) from pore fluid chloride concentrations.

Core #	Depth (mbsf)	$[Cl]_{obs}$ (mM)	$[Cl]_{fit}$ (mM)	S_h (%)	Core #	Depth (mbsf)	$[Cl]_{obs}$ (mM)	$[Cl]_{fit}$ (mM)	S_h (%)
SE seepage:GeoB21619-1	3.35	633.5	634.8	<1	SW seepage:	5.80	429.6	584.2	31
	3.51	512.3	637.8	24	GeoB21637-1	6.28	454.1	587.1	27
	3.61	591.2	639.7	9		6.42	471.0	588.1	24
	3.90	376.4	645.1	47		6.54	520.9	589.1	14
	4.00	608.9	647.0	7		6.90	514.9	592.1	16
	4.34	483.8	653.3	31		7.11	543.9	594.1	10
	4.43	490.7	655.0	30		7.38	555.9	596.8	9
	4.53	475.9	656.9	32		8.28	534.9	608.3	15
	4.63	417.8	658.7	42		10.29	456.6	648.3	35
	4.73	537.0	660.6	22		10.88	584.8	664.4	15
Lomvi-seepage:	2.38	552.5	593.9	13		11.29	556.9	677.4	21
GeoB21624-1	2.62	578.8	597.3	4		11.54	607.8	685.8	14
GeoB21623-1	1.54	541.8	580.0	8	GeoB21621-1	6.51	424.1	588.9	32

3.2. Downcore variation in pore water composition

We report the downcore concentration profiles of dissolved sulfate and chloride as well as pore water B/Cl ratios, $\delta^{11}B$, $\delta^{18}O$, and δD to investigate the sources of fluid and gas hydrate dynamics. All pore water data were compiled based on the coring locations and presented in Fig. 2. Dissolved sulfate concentrations decrease rapidly from a seawater value (28 mM) towards the sulfate-methane-transition (SMT), which is defined by the shallowest depths where significant amounts of methane can be detected and sulfate concentrations drop to a sub-millimolar level (Fig. 2a, 2e, 2h, 2m and 2s). SMT depths range from *ca.* 10 mbsf at the reference site, 2.5 mbsf in the non-seepage site and less than one mbsf for the seepage sites (Fig. 2). A few millimolar sulfate can still be observed in the deeper sediments, which is a sign for the contamination by seawater during core recovery and handling (Bohrmann et al., 2017; Pape et al., 2020).

We report pore water B/Cl ratios, instead of absolute concentrations of dissolved boron, to correct for the effect of gas hydrate dissolution and formation. Pore water B/Cl ratio profiles from the reference site and the non-seepage site in the Lunde pockmark exhibit downcore decreasing trends in general from 9×10^{-4} mol/mol close to the sediment-water interface to ca. 6×10^{-4} mol/mol at the bottom of the sites (Fig. 2c and 2g). In the Lunde SE seepage site, pore water B/Cl ratios are fairly constant with depth (ca. 8×10^{-4} mol/mol) except for the two anomalous values (around 9×10^{-4} mol/mol) from the hydrate-bearing interval (3.35–4.73 mbsf, Fig. 2i). In the Lunde SW seepage site, pore water B/Cl ratios slightly decrease with depth from 8×10^{-4} mol/mol close to the sediment-water interface to 6×10^{-4} mol/mol at four mbsf and increase abruptly within the two hydrate-bearing horizons (5.80–8.28 mbsf and 10.29 to 11.54 mbsf) with ratios as high as 9×10^{-4} mol/mol (Fig. 2o). From the Lomvi pockmark, pore water B/Cl ratios decrease with depth within the uppermost 2.5 m of sediments from 8×10^{-4} mol/mol close to the sediment-water interface to 5×10^{-4} mol/mol at 2.5 mbsf. Only the two samples from 2.56 to 2.62 mbsf show anomalous pore water B/Cl ratios as high as 9×10^{-4} mol/mol (Fig. 2u).

The $\delta^{11}B$ in pore water were measured for samples from the reference and the Lunde SW seepage sites as well as from Lomvi pockmark sites. The $\delta^{11}B$ profile from the reference site shows a slight decreasing trend from the expected seawater value of +39.6‰ at seafloor to +37.0‰ at five mbsf and an increase with depth to +41.0‰ between five mbsf and the bottom of the core (*ca.* 60 mbsf) with a few fluctuations in between (Fig. 2d). From the Lunde SW seepage site, the $\delta^{11}B$ values also slightly decrease from the expected seawater value at seafloor to +37.0‰ at four mbsf (Fig. 2p). The values increase to +39.5‰ at 15.11 mbsf with low values (+35.0‰ to +37.5‰) within the intervals where gas hydrates were recovered (Fig. 2p). A slight decrease in $\delta^{11}B$ values with depth (from +39.0‰ to +37.0‰) was observed from the four available measurements in the top 2.62 m in the Lomvi pockmark cores (Fig. 2v). The two gas hydrate samples have $\delta^{11}B$ values of +26.5‰ and +30.3‰ that are significantly lower than all the values from pore fluid samples investigated.

Downcore [Cl] at the Lunde reference and the non-seepage sites show small variations ranging between 540 and 560 mM (Fig. 2b and 2f). Larger variations in the [Cl] (424.1–890.7 mM) were observed from the Lunde SW and SE seepage sites as well as from the Lomvi seepage site (Fig. 2i, 2n and 2t and Table 2). The [Cl] at the Lunde SE seepage site show a gradual increase in the uppermost three m of sediments from 572.4 mM to 618.8 mM. In the hydrate-bearing sediments below three mbsf, [Cl] fluctuate between 376.4 mM and 608.9 mM. The [Cl] profile from the Lunde SW seepage site shows a more complicated structure. The range of [Cl] from the hydrate-free sediments for the uppermost six m of sediments is fairly narrow (575.4 mM–591.3 mM) with a pronounced downcore increase observed from *ca.* 6 mbsf to 15.11 mbsf (528.8 mM–890.7 mM, respectively). For the samples taken from the two hydrate-bearing intervals of this site, [Cl] fluctuate between 424.1 mM and 607.8 mM. At the Lomvi seepage site, [Cl] show a general downcore increasing trend with anomalously low values down to 541.8 mM in the three sediment horizons where gas hydrates were recovered (1.54, 2.38, and 2.62 mbsf; Fig. 2t & Table 2).

$\delta^{18}O$ and δD were analyzed for seepage sites in the Lunde and Lomvi pockmarks. At the Lunde SE seepage site, the values of both isotopes decrease slightly with depth from +0.2‰ to 0‰ for $\delta^{18}O$ and −0.1‰ to −0.5‰ for δD within the uppermost 3 m of hydrate-free sediments (Fig. 2k and l). Water samples taken from the hydrate-bearing samples deeper than 3.35 mbsf at this site have values up to +1.1‰ and +7.9‰ for $\delta^{18}O$ and δD, respectively (Fig. 2k and 2l). At the Lunde SW seepage site, the downcore $\delta^{18}O$ and δD profiles also exhibit complex structures with relatively little fluctuation in values above six mbsf and high values observed in the two hydrate-bearing intervals (Figs. 2q and 2r). Between six and ten mbsf the isotopic values gradually increase with depth in the hydrate-free sediments and decrease towards lower values (+0.3‰ for $\delta^{18}O$ and +1.8‰ for δD) in the deepest three samples (14.74–15.12 mbsf: Figs. 2q and 2r). In general, there are relatively smaller changes in both $\delta^{18}O$ and δD signatures from the Lomvi seepage site. Only one sample at 2.38 mbsf shows slightly higher $\delta^{18}O$ (+0.5‰) and δD values (+2.4‰) as compared to values for bottom seawater (Figs. 2w and 2x).

4. Discussion

4.1. Pore water sources inferred from chloride concentration, $\delta^{18}O$ and δD

We investigate the sources of water and processes that contribute to the observed changes in fluid composition from the Lunde seepage sites by studying the profiles of [Cl], $\delta^{18}O$ and δD. We compared our data ($[Cl]_{obs}$, $\delta^{18}O_{obs}$ and δD_{obs}) with values of assigned references ($[Cl]_{ref}$, $\delta^{18}O_{ref}$ and δD_{ref}) to investigate the effect of fluid mixing and gas hydrate dynamics (Fig. 3). We chose two sets of reference composition: modern seawater (Lunde SE seepage site) and the composition of a sample from 8.78 mbsf (Lunde SW seepage site) for reasons discussed below.

Following the approach developed by Tomaru et al. (2006), we defined the normalized chloride concentrations, *f*, as the ratios between the observed and reference dissolved chloride concentrations (i.e. $[Cl]_{obs}/[Cl]_{ref}$; Fig. 3). The *f* values reflect the mixing of fluids with different [Cl]. The *f* values larger than one indicate consumption of fresh water through processes such as gas hydrate formation, while values smaller than one refer to fresh water addition through processes such as gas hydrate decomposition. We also defined parameters that describe the differences between the observed and reference isotopic signatures of water as $\Delta\delta^{18}O$ ($= \delta^{18}O_{obs} - \delta^{18}O_{ref}$) and $\Delta\delta D$ ($= \delta D_{obs} - \delta D_{ref}$) (Fig. 3). Gas hydrate formation is known to preferentially concentrate ^{18}O and ^{2}H in the hydrate lattice, which results in lower $\delta^{18}O$ and δD values in the residual fluids (Maekawa, 2004). The degree of such isotopic fractionation can be quantified experimentally and expressed as isotopic fractionation factors (α_O = 1.0023 to 1.0034 and α_H = 1.014 to 1.024; Maekawa (2004)) assuming Rayleigh-type fractionation in a closed system. The values of α were derived by knowing the heavy-to-light isotopic ratios (*R*) between the final and initial solutions as well as the fraction of water from gas hydrate in the final solution (see Maekawa, 2004 for more detail). During gas hydrate decomposition, the release of ^{18}O- and ^{2}H-enriched fresh water from hydrate lattice results in higher $\delta^{18}O$ and δD values of the pore water.

When analyzing the pore fluid data with this approach, all the data from the Lunde SE seepage site can be well explained when modern seawater composition was chosen as the reference ($[Cl]_{ref}$: 574 mM; $\delta^{18}O_{ref}$: +0.2‰; δD_{ref}: −0.1‰) (Fig. 3a and 3b). The data from hydrate-bearing samples can be explained as the buried seawater modified by gas hydrate dissociation during core recovery. The downcore increase in $[Cl]_{obs}$ (up to 633 mM) from the hydrate-free samples at this site may hint to ongoing gas hydrate formation. However, this inference is only marginally supported by the $\delta^{18}O_{obs}$ and δD_{obs} signatures as the pore

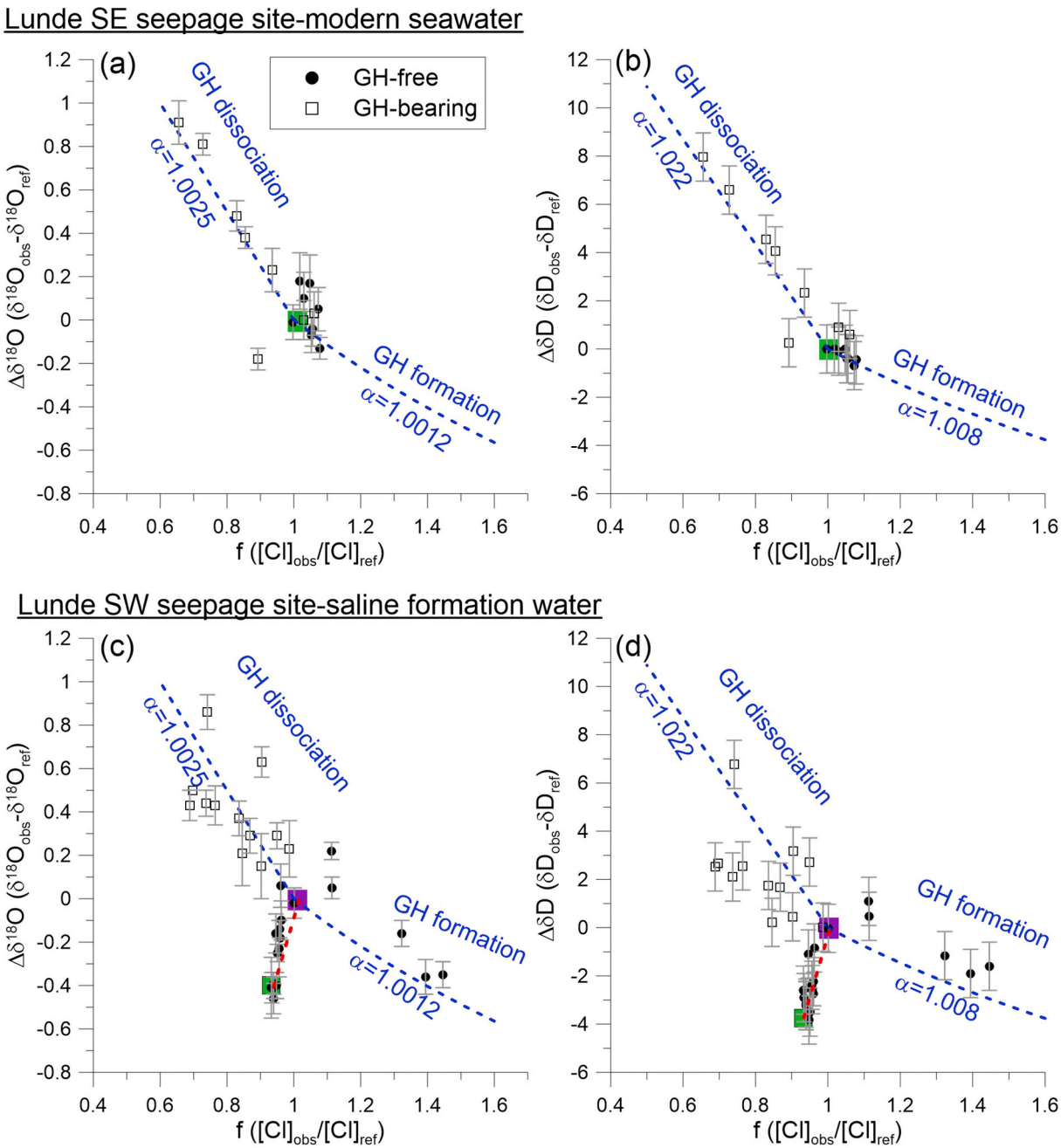

Fig. 3. Normalized chloride concentration (*f*) versus differences in $\delta^{18}O_{obs}$ (Fig. 3a and 3c) and δD_{obs} (Fig. 3b and 3d) relative to the assigned reference composition ($\Delta\delta^{18}O$ and $\Delta\delta D$) (GH = gas hydrate). The uncertainty in *f* is smaller than the symbol size as [Cl] is precisely determined through titration. For the Lunde SE seepage site (Fig. 3a and 3b), we chose modern seawater composition as the reference (green squares; $[Cl]_{ref} = 574$ mM, $\delta^{18}O_{ref} = +0.20‰$, $dD_{ref} = -0.06‰$). Most of the data from hydrate-bearing samples can be explained by the expected fractionation factors (α) for gas hydrate dissociation and formation determined from laboratory experiments (e.g., Maekawa 2004). For the Lunde SW seepage site (Fig. 3c and 3d), we chose the composition from a sample at 8.78 mbsf as the reference (purple squares; $[Cl]_{ref} = 616$ mM, $\delta^{18}O_{ref} = +0.60‰$, $\delta D_{ref} = +3.76‰$) as modern seawater composition fails to explain the distribution of data (see Suppl. Fig. 1). We propose that the values of the sample at 8.78 mbsf represent the composition of a saline formation fluid that, in addition of mixing with local bottom seawater (red dash lines), was modified by hydrate formation at greater depths and gas hydrate dissociation during core recovery. (For interpretation of the references to colour in this figure legend, the reader is referred to the Web version of this article.)

water sample from 2.53 mbsf, where the deepest hydrate-free sediment sample were obtained, are only slightly depleted in ^{18}O and ^{2}H. In addition, $\delta^{18}O_{obs}$ and δD_{obs} signatures from samples deeper than 2.53 mbsf were affected by hydrate dissociation during core recovery and thus cannot be used to infer any likely formation of gas hydrate.

In contrast, the changes in $\delta^{18}O_{obs}$ and δD_{obs} from the Lunde SW seepage sites cannot be explained with hydrate dynamics if the composition of modern seawater is assigned as the reference (Suppl. Fig. 1). Instead, the data can be better fitted when the composition of the sample from 8.78 mbsf is used as the reference ($[Cl]_{ref}$: 616 mM, $\delta^{18}O_{ref}$: +0.6‰, δD_{ref}: +3.8‰) (Fig. 3c and 3d). This composition hints to the presence of a saline formation fluid that, when compared to modern seawater, it has higher [Cl] by 42 mM as well as higher $\delta^{18}O$ and δD values by 0.4‰ and 3.8‰, respectively. Between seafloor and 5.80 mbsf, [Cl], $\delta^{18}O$ and δD reflect mixing between this saline formation water and modern bottom seawater (red dash lines in Fig. 3c and 3d). Between 5.80 and 11.54 mbsf, this saline formation water was modified by gas hydrate dissociation during core recovery (open squares in Fig. 3c and d), which results in $\Delta\delta^{18}O$ and $\Delta\delta D$ values up to 1.0‰ and 7.0‰, respectively. Below 11.54 mbsf, the enrichment in [Cl] up to 890 mM as well as $\delta^{18}O_{obs}$ and δD_{obs} similar to modern seawater values can be best explained by the saline formation water modified by active gas hydrate formation, even though there is no gas hydrate recovered (closed circles in Fig. 3c and 3d).

We propose that this saline formation water originated from old evaporated seawater that was buried with the strata at great depths. Though not without uncertainties, this explanation is supported by the overall similar Br/Cl ratios between our pore fluid samples and seawater (Suppl. Fig. 2). An alternative explanation for the high [Cl], $\delta^{18}O$ and δD of the proposed saline fluid is the residual fluids after clay ion filtration, which leads to the enrichments of anion as well as high $\delta^{18}O$ and δD values (Phillips and Bentley 1987). This process however fails to explain why the same saline formation water is not observed from other sites investigated (e.g., Lunde non-seep and reference sites, Fig. 2), which should all be situated in a similar clay mineral composition. Authigenic clay formation is also known to result in residual fluids with high [Cl] (Kastner et al., 1991; Sheppard and Gilg 1996; Dählmann and De Lange 2003). This explanation can however be ruled out as clay formation fractionates $\delta^{18}O$ and δD in opposite directions (Kastner et al., 1991; Sheppard and Gilg 1996; Dählmann and De Lange 2003) and cannot explain the high values in both $\delta^{18}O$ and δD of this saline formation fluid from the Lunde SW seepage site.

4.2. Modes of gas hydrate formation controlled by methane supply

The flux of methane as well as the composition of the fluid, such as salinity, are two of the most important factors that determine gas hydrate abundance. When combining the knowledge of downcore variations of gas hydrate abundance and the time scales of local methane seepage, as derived from the authigenic carbonate records (e.g., Himmler et al., 2019), one could investigate the different modes of gas hydrate formation. We estimated S_h up to 35% pore space from the two hydrate-bearing horizons in the Lunde SW seepage site based on the $[Cl]_{obs}$ (Fig. 2n and Table 2). At the Lunde SE seepage site and the Lomvi seepage site the maximum S_h is 47% and 13%, respectively (Fig. 2i, 2t and Table 2). Our estimation is much higher than that derived from waveform inversion modeling of ocean-bottom seismic (OBS) (0–2% pore space in the upper 50 m of sediments from Singhroha et al., 2019), but similar to the estimation based on controlled source electromagnetic (CSEM) (*ca.* 30% pore space; Goswami et al., 2017) from Vestnesa Ridge. We acknowledge that part of the differences can be attributed to the different methods used (geophysical vs. geochemical), different physical scales focused by these methods, and the locations where these measurements were performed (*i.e.* ridge crest vs. flank) with the OBS stations located outside the pockmark footprint and the CSEM transmitter being towed along the ridge. Nonetheless, while the OBS estimation may represent a gas hydrate distribution under a diffusive flow system (Singhroha et al., 2019), our results and the CSEM estimation likely represent the saturation from the chimney where gas hydrate formation is actively sustained by focused gaseous methane supplied through fractures (Pape et al., 2020). We however note that these geophysical methods are not able to differentiate free gas from gas hydrate (Singhroha et al., 2020). Therefore, direct comparison of hydrate saturation may be problematic.

We are able to differentiate the status of gas hydrate deposits, namely active formation versus dynamic equilibrium under ambient pressure and temperature conditions. It has been shown from Hydrate Ridge, Cascadia Margin (NE Pacific Ocean), and Ulleung Basin (Sea of Japan or East Sea) that positive chloride concentration anomalies are not necessarily associated with all hydrate deposits (see Hong and Peszynska 2018 for a review of data from these locations). When hydrate formation slows down, deposits of gas hydrate can reach a status of dynamic equilibrium. In other words, there is no net gain or loss of gas hydrate under such equilibrium status as hydrate formation is as fast as its dissolution. The supply of methane is only high enough to maintain the dissolved methane concentration at a saturation level and compensate for methane loss via diffusion and microbial consumption (e.g., anaerobic oxidation of methane, Boetius et al., 2000), but too low to support additional hydrate formation. Dissolved chloride that is expelled during an early stage of active formation slowly diffuses away under the dynamic equilibrium.

Hong and Peszynska (2018) applied a kinetic model on the data obtained from IODP Site1328 (Cascadia Margin). They showed that the gas hydrate deposits not associated with positive chloride concentration anomalies could be explained by either a slow formation or periodically fast formation with a prolonged relaxation period. In the former explanation, the rates of hydrate formation would be only slightly higher than that under dynamic equilibrium which takes a time scale of 250,000 years (250 thousand years or 250 kyr) to form 40% (pore space) of gas hydrate. The dissolved chloride that is expelled during hydrate formation has sufficient time to diffuse away and results in no accumulation of chloride in the pore water. For the periodically fast formation with a prolonged relaxation period, massive gas hydrate can form in a very short period of time (200 years for 40% of gas hydrate in pore space) sustained by pulses of methane gas supply. The rapid formation is followed by a prolonged relaxation stage (40 kyr for the gas hydrates at 233 mbsf from IODP Site1328) that allows sufficient time for the large positive chloride concentration anomalies to diffuse away.

The temporal constraints obtained from U–Th dating of seep carbonates from the Lunde SW seepage site allow us to further differentiate the two hydrate formation modes from this site. The U–Th ages from seep carbonates suggest two major past seepage events at the Lunde SW seepage site: 40–50 thousand years ago (ka) (determined from 5 to 10 mbsf at MeBo drill site GeoB21616-1) and 133–160 ka (determined from >15 mbsf from MeBo drill site GeoB21637-1; Fig. 1b) (Himmler et al., 2019). Based on these carbonate age inferences, the event-driven rapid hydrate formation is a more likely scenario as the slow hydrate formation requires a minimum formation time that exceeds the ages of seep carbonates and hosting formation (*i.e.,* 250 kyr to built-up 40% of gas hydrates as estimated by Hong and Peszynsk (2018)). As the gas hydrate recovered from the Lunde SW seepage site is notably shallower (<11.54 mbsf; Table 2) than that at IODP Site1328, the length of time required for the positive chloride concentration anomalies to mix with seawater is expected to be significantly shorter than 40 kyr from this site. To form gas hydrate within a few centuries under the periodically fast hydrate formation condition, a large upward flux of methane gas is required, a conclusion supported by previous studies (Haeckel et al., 2004; Torres et al., 2004; Liu and Flemings 2006; Sultan et al., 2014; Hong et al., 2018), and by the bubble fabric in the gas hydrate pieces recovered (Fig. 1c) (Bohrmann et al., 1998; Sultan et al., 2014). Even though the recovered gas hydrates from the Lunde SW seepage site likely formed during periods of intensive gas seepage events in the past, the absence of

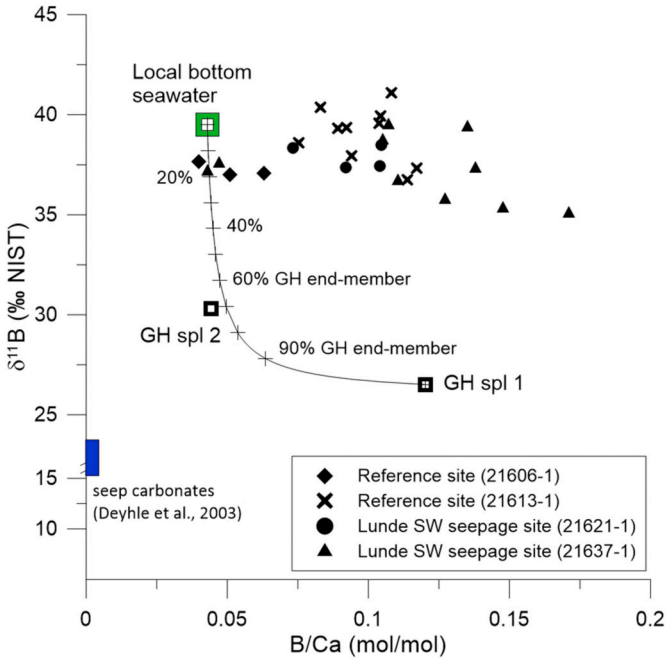

Fig. 4. A mixing diagram between local bottom seawater (open green square) and water from gas hydrate as represented by the composition of gas hydrate sample 1 (GH spl 1; open black square). The GH spl 2 with higher $\delta^{11}B$ signature (as compared to the value from GH sp1) can be explained by ca. 30% mixing from local bottom seawater, likely as a result of contamination during sampling. Neither gas hydrate dissociation nor seep carbonates dissolution (blue square) can explain the observed boron signatures from pore fluids (cross, solid triangle, and circle). This observation supports the inference that the pore fluid boron signatures reflect in-situ signal from a deeply-buried fluid source. (For interpretation of the references to colour in this figure legend, the reader is referred to the Web version of this article.)

positive [Cl] anomalies associated with them (Fig. 2n) suggests that these gas hydrates have reached a status of dynamic equilibrium that their formation is as fast as decomposition.

4.3. Migration of saline fluid from deep formations inferred from stable boron isotopic signatures

In the previous sections, we show that [Cl], $\delta^{18}O$ and δD signatures from the Lunde SW seepage site can be best explained by a saline formation fluid mixed with modern seawater and modified by gas hydrate dynamics. We propose that such a saline formation fluid originated from much greater depths and its flow conduit was intercepted at the SW seepage site, an inference supported by the B/Cl molar ratios and $\delta^{11}B$ of pore water.

In the hydrate-free sediments from the Lunde SW seepage and reference sites, pore water samples have lower B/Cl ratios (down to 6×10^{-4} mol/mol, Fig. 2c and 2o) and $\delta^{11}B$ signatures (+38.0‰ to +40.0‰, Fig. 2d and 2p) as compared to the seawater values. Pore fluids in these sediments are not influenced by any deep-rooted fluids but were affected by a combination of local diagenetic processes. For example, Hüpers et al. (2016) interpreted the low pore fluid boron concentrations and $\delta^{11}B$ signatures observed from Nankai Trough as the results of combined effect from volcanic ash alteration and NH_4-induced boron desorption from clay surface. Though there is no volcanic ash reported from Vestnesa Ridge, we expect a similar combination of processes to occur and explain the observed profiles. On the other hand, the co-occurrence of high pore fluid B/Cl ratios (up to 8×10^{-4} mol/mol or 43% higher than that of bottom seawater ratio) and $\delta^{11}B$ as low as +35.0‰ in the pore fluid observed from the hydrate-bearing samples in SW seepage site indicates a deep-rooted fluid that has received boron desorbed from clay surfaces under sufficiently high temperatures (Palmer et al., 1987). Similar boron signals have been observed along the decollement fault from several accretionary prism systems and used to infer upward migration of crustal fluids (You et al., 1995a, b).

Low $\delta^{11}B$ values (+15.6‰ to +22.9‰) were also reported for seep carbonates from the mud volcano in the eastern Mediterranean Sea (Deyhle et al., 2003). Carbonate dissolution or re-crystallization may therefore release boron with low $\delta^{11}B$ values into the pore water. However, the low B/Ca ratios observed from the Mediterranean seep carbonates (in the range of 29.7–167.0 μmol/mol; Deyhle et al., 2003) make this process unlikely to explain the elevated B/Ca ratios observed in our pore water samples (Fig. 4). In addition, there is no sign of significant calcium carbonate dissolution from the SW seepage site based on the absence of downcore variation in Ca/Cl ratios below the SMT (Suppl. Fig. 2).

Kopf et al. (2000) suggested that water from gas hydrate decomposition is depleted in ^{11}B ($\delta^{11}B = +30.6‰$) and may lower the $\delta^{11}B$ values in pore fluids. This hypothesis was challenged by later studies (e.g., Teichert et al., 2005; Hüpers et al., 2016) that suggested a limited effect of gas hydrate dissociation on $\delta^{11}B$ of the pore fluids. We evaluate this hypothesis by considering a binary mixing between modern seawater and a gas hydrate-derived end member represented by one of our gas hydrate samples with a $\delta^{11}B$ value of +26.5‰ (GH spl 1; Fig. 4). While the $\delta^{11}B$ value of the other gas hydrate sample (GH spl 2; +30.3‰) can be explained by the mixing of bottom seawater and our assigned gas hydrate end member, the mixing trend fails to explain the values for other pore fluid samples (Fig. 4). It is apparent that pore water B/Ca ratios are insensitive to mixing with water released from dissociating gas hydrate as this solution is characterized by low calcium and boron concentrations (0.4–0.7 mM for calcium and 31.3–49.5 μM for boron). For example, a *ca.* 34% mixing with the gas hydrate end member is able to explain the lowest $\delta^{11}B$ value observed from our pore fluid samples even though the resulting B/Ca ratios are only 3.4% higher than the modern seawater B/Ca ratio (Fig. 4). We can therefore exclude the influence of gas hydrate dissociation on the pore fluid boron signals and conclude that both porewater $\delta^{11}B$ and B/Ca ratios indicate a deep-rooted fluid under modification of high-temperature diagenesis.

4.4. Interaction between fluid flow and shallow gas hydrate dynamics from the Lunde pockmark

The pore fluid geochemistry from the Lunde SW seepage site hints to a saline formation water modified by high-temperature diagenesis. This formation water supplies the sediment with barely sufficient methane to maintain the two gas hydrate deposits at dynamic equilibrium, which is inferred from the lack of positive [Cl] anomaly associated with the gas hydrates recovered. We integrate these findings with previous studies from the Lunde pockmark and propose an evolution model for the fluid pumping systems (Fig. 5). The internal structure of a gas chimney is highly complex with fractures and zones of low permeability materials (e.g., gas hydrates and carbonates) that influence the migration pathways of ascending fluids (e.g., Gay et al., 2011 and Sultan et al., 2014). Based on the high resolution 3-D P-cable seismic data, Plaza-Faverola et al. (2015) documented buried mounds at several seismic horizons (e.g., H50 in Fig. 5c) along the Vestnesa Ridge. One of these buried features observed in seismic data beneath the Lunde pockmark was correlated with the carbonates-cemented sediments recovered from the Lunde SW seepage site and confirmed to be an indication of a past seepage event (see Fig. 5b and Himmler et al., 2019). These carbonate-cemented sediments formed as a result of the alkalinity increase during anaerobic oxidation of methane gradually blocked the primary conduits for fluid flow, such as what happened beneath the main depression of the Lunde pockmark (the buried pockmarks/seep carbonate in Fig. 5a that corresponds to ca. 1.75 s two-way travel time in Fig. 1d). As a result, the flow was diverted from the main depression and flowed southwesterly towards the SW seepage site (Fig. 5a) as well as the SE part of the

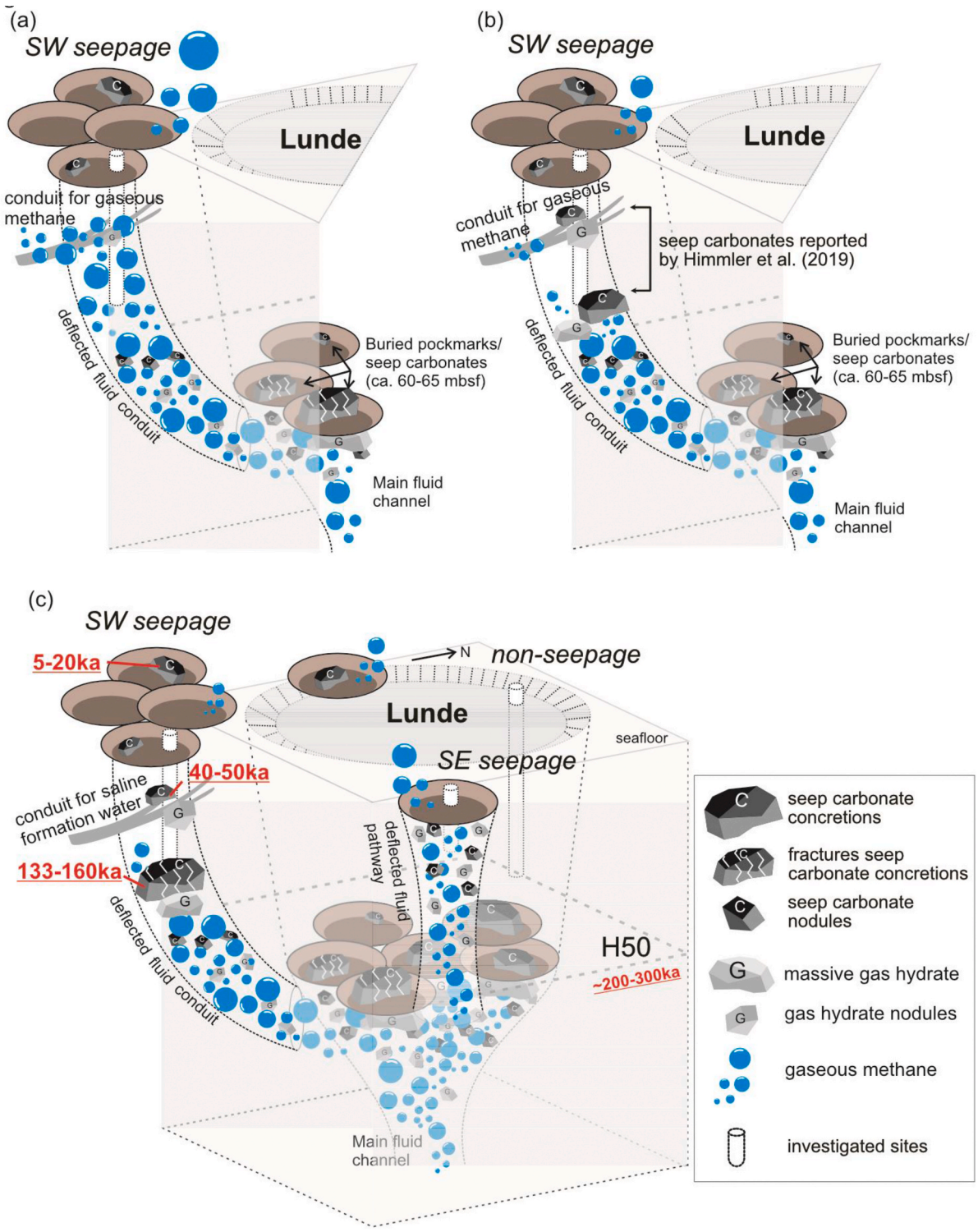

Fig. 5. A conceptual evolution model for the fluid pumping system of Lunde pockmark that integrates seismic interpretation, U–Th ages of seep carbonates and the pore fluid geochemistry. (a) When the main fluid channel was blocked by the buried pockmarks/seep carbonates observed from the seismic profile (corresponds to the H50 horizon in Fig. 1d), a deflected fluid conduit was created which directed the fluid flow towards the SW seepage site. Gaseous methane was diverted and forced to flow along this conduit, which triggered active formation of gas hydrate that was recovered in this study. (b) The fluid conduit was gradually blocked by the seep carbonate cementation, which also decreases the gas discharge on the seafloor through this conduit. (c) At the present day, the dynamic equilibrium status of the gas hydrates from the SW seepage site suggests a halt of gaseous supply, likely due to the complete blockage by the carbonate cemented sediments that were recovered during drilling (Fig. 1c). The saline formation water is still able to migrate along the same fluid conduit used by gaseous methane in the past. Signs of active hydrate formation can be observed in the pore fluid from the bottom of the soft sediments recovered at SW seepage site. This hints to an active formation of gas hydrate in the laterally or horizontally adjacent sediments. The active fluid seepage and hydrate formation from SE seepage site indicate the genesis of a new deflected conduit from this location (similar to the SW seepage site in (a)). Age data of seep carbonates that are associated with previous methane seepage events were determined by the U–Th method (Himmler et al., 2019), while the age of H50 horizon was determined by local sedimentation rates (Knies et al., 2014; Mattingsdal et al., 2014).

pockmark (*i.e.* SE seepage site) (Fig. 5c). Such a mechanism explains why only low to moderate methane fluxes can be inferred from the pore fluid profiles of the Lunde non-seepage site (Figs. 1 and 5 for location and quantification from Pape et al., 2020). The gas hydrates recovered from the SW seepage site formed during a period of seepage with high gaseous methane supply (i.e. Fig. 5a and 5b), as indicated by the bubble fabric observed (Fig. 1c). Such gaseous methane supply gradually diminished as a result of the formation of carbonate crusts that were recovered at the SW seepage site (Fig. 5b). Such a mechanism has been proposed through numerical modeling (e.g., Luff et al., 2004; Luff et al., 2005) and the investigations of seep carbonates texture along the Norwegian margin (Hovland et al., 2002; Mazzini et al., 2003). Despite the partly blocked fluid conduit, the same fluid conduit still connects to a deep sourced aqueous fluid. Dissolved methane and other pore fluid constituents are able to reach the shallow sub-surface through diffusion, as reflected by the presence of saline formation water and boron anomalies. The lack of [Cl] positive anomalies associated with these gas hydrates supports the inference of a weaker methane supply as the gas hydrates are currently in a dynamic equilibrium status with formation as fast as its decomposition (Fig. 5c).

5. Conclusions

The pockmarks along Vestnesa Ridge have been excellent field laboratories for the studies of fluid migration and gas hydrate dynamics along the passive continental margins. Multi-disciplinary approaches integrating the knowledge of fluid geochemistry, geology, and geophysics, similar to what is achieved in this work, are critical for a holistic understanding of the system. With the access to sediment and samples tens of meters below seafloor, we are able to constrain the source of fluids and processes that modify fluid composition. The transition from brief but strong gaseous methane seepage episodes to a state of low diffusive methane supply is inferred from the presence of gas hydrate deposits without cooccurring positive chloride concentration anomalies. Such a transition is likely the result of fluid divergence by seep carbonates that were formed during the strong seepage periods but are now buried deep in the sediment sequence. The presently low methane flux is sustained by the flow of a saline formation fluid that originated from great depths. Our findings highlight the importance of conduit quality and fluid phase in controlling the migration of methane as well as the dynamics of gas hydrates in pockmarks.

Credit author statement

Hong W.-L., Conceptualization, Formal analysis, Investigation, Writing – original draft, Visualization. Pape T., Validation, Formal analysis, Investigation, Writing – review & editing. Schmidt C., Formal analysis, Investigation, Writing – review & editing. Yao H., Formal analysis, Investigation. Wallmann K., Formal analysis, Investigation, Writing – review & editing, Supervision. Plaza-Faverola A., Formal analysis, Investigation, Writing – review & editing. Rae J.W.B., Methodology, Writing – review & editing. Lepland A., Methodology, Writing – review & editing. Bünz S., Writing – review & editing, Supervision, Project administration, Funding acquisition. Bohrmann G., Writing – review & editing, Supervision, Project administration, Funding acquisition.

Declaration of competing interest

The authors declare that they have no known competing financial interests or personal relationships that could have appeared to influence the work reported in this paper.

Acknowledgments, Samples, and Data

We acknowledge the crews and captain from R/V 'MARIA S. MERIAN' as well as the MeBo team and the cruise participants during cruise MSM57-1/-2. Cruise MSM57-1/-2 was funded by the German Research Foundation (DFG), the Research Center/Excellence Cluster "The Ocean in the Earth System" at MARUM–Center for Marine and Environmental Sciences, University of Bremen and funds from CAGE. This work is partly supported by the Research Council of Norway (RCN) through Petromaks2-NORCRUST (project number 255150) and the Centre of Excellence funding scheme for CAGE (project number 223259). APF's contribution was part of the SEAMSTRESS project supported by starting grants from the Tromsø Research Foundation and the Research Council of Norway (grant nr. 2878659). The pore fluid data reported can be found from the Data Center PANGAEA (https://doi.pangaea.de/10.1594/PANGAEA.918039).

Appendix A. Supplementary data

Supplementary data to this article can be found online at https://doi.org/10.1016/j.marpetgeo.2021.104957.

References

Boetius, A., Ravenschlag, K., Schubert, C.J., Rickert, D., Widdel, F., Gieseke, A., Amann, R., Jorgensen, B.B., Witte, U., Pfannkuche, O., 2000. A marine microbial consortium apparently mediating anaerobic oxidation of methane. Nature 407 (6804), 623–626.

Bohrmann, G., Ahrlich, F., Bergenthal, M., Bünz, S., Düßmann, R., Ferreira, C., Freudenthal, T., Fröhlich, S., Hamann, K., Hong, W.-L., Hsu, C.-W., Johnson, J., Kaszemeik, K., Kausche, A., Klein, T., Lange, M., Lepland, A., Malnati, J., Meckel, S., Meyer-Schack, B., Noorlander, K., Panieri, G., Pape, T., Reuter, M., Riedel, M., Rosiak, U., Schmidt, C., Schmidt, W., Seiter, C., Spagnoli, G., Stachowski, A., Stange, N., Wallmann, K., Wintersteller, P., Wunsch, D., Yao, H., 2017. R/V MARIA S. MERIAN cruise report MSM57, gas hydrate dynamics at the continental margin of Svalbard, Reykjavik – Longyearbyen – Reykjavik. In: Berichte, MARUM – Zentrum für Marine Umweltwissenschaften. Fachbereich Geowissenschaften, Universität Bremen, Bremen.

Bohrmann, G., Greinert, J., Suess, E., Torres, M., 1998. Authigenic carbonates from the Cascadia subduction zone and their relation to gas hydrate stability. Geology 26 (7), 647–650.

Bünz, S., Polyanov, S., Vadakkepuliyambatta, S., Consolaro, C., Mienert, J., 2012. Active gas venting through hydrate-bearing sediments on the Vestnesa Ridge, offshore W-Svalbard. Mar. Geol. 332–334, 189–197.

Chen, N.-C., Yang, T.F., Hong, W.-L., Yu, T.-L., Lin, I.-T., Wang, P.-L., Lin, S., Su, C.-C., Shen, C.-C., Wang, Y., 2020. Discharge of deeply rooted fluids from submarine mud volcanism in the Taiwan accretionary prism. Sci. Rep. 10 (1), 1–12.

Dählmann, A., De Lange, G., 2003. Fluid–sediment interactions at Eastern Mediterranean mud volcanoes: a stable isotope study from ODP Leg 160. Earth Planet Sci. Lett. 212 (3–4), 377–391.

Deyhle, A., Kopf, A., 2001. Deep fluids and ancient pore waters at the backstop: stable isotope systematics (B, C, O) of mud-volcano deposits on the Mediterranean Ridge accretionary wedge. Geology 29 (11), 1031–1034.

Deyhle, A., Kopf, A.J., Aloisi, G., 2003. Boron and boron isotopes as tracers for diagenetic reactions and depth of mobilization, using muds and authigenic carbonates from eastern Mediterranean mud volcanoes. Geol. Soc. Londn. Special Publ. 216 (1), 491–503.

Foster, G., 2008. Seawater pH, pCO_2 and $[CO_2^{-3}]$ variations in the Caribbean Sea over the last 130 kyr: a boron isotope and B/Ca study of planktic foraminifera. Earth Planet Sci. Lett. 271 (1–4), 254–266.

Foster, G.L., Hönisch, B., Paris, G., Dwyer, G.S., Rae, J.W., Elliott, T., Gaillardet, J., Hemming, N.G., Louvat, P., Vengosh, A., 2013. Interlaboratory comparison of boron isotope analyses of boric acid, seawater and marine $CaCO_3$ by MC-ICPMS and NTIMS. Chem. Geol. 358, 1–14.

Freudenthal, T., Wefer, G., 2013. Drilling cores on the sea floor with the remote-controlled sea floor drilling rig MeBo. Geosci. Instrument. Methods Data Syst. 2 (2), 329–337.

Gay, A., Takano, Y., Gilhooly III, W.P., Berndt, C., Heeschen, K., Suzuki, N., Saegusa, S., Nakagawa, F., Tsunogai, U., Jiang, S.Y., Lopez, M., 2011. Geophysical and geochemical evidence of large scale fluid flow within shallow sediments in the eastern Gulf of Mexico, offshore Louisiana. Geofluids 11 (1), 34–47.

Goswami, B.K., Weitemeyer, K.A., Bünz, S., Minshull, T.A., Westbrook, G.K., Ker, S., Sinha, M.C., 2017. Variations in pockmark composition at the Vestnesa Ridge: insights from marine controlled source electromagnetic and seismic data. Geochem. Geophys. Geosystem 18 (3), 1111–1125.

Haeckel, M., Suess, E., Wallmann, K., Rickert, D., 2004. Rising methane gas bubbles form massive hydrate layers at the seafloor. Geochem. Cosmochim. Acta 68 (21), 4335–4345.

Hesse, R., 2003. Pore water anomalies of submarine gas-hydrate zones as tool to assess hydrate abundance and distribution in the subsurface - what have we learned in the past decade? Earth Sci. Rev. 61 (1–2), 149–179.

Himmler, T., Sahy, D., Martma, T., Bohrmann, G., Plaza-Faverola, A., Bünz, S., Condon, D.J., Knies, J., Lepland, A., 2019. A 160,000-year-old history of tectonically controlled methane seepage in the Arctic. Sci. Adv. 5 (8), eaaw1450.

Hong, W.-L., Lepland, A., Himmler, T., Kim, J.-H., Chand, S., Sahy, D., Solomon, E.A., Rae, J.W., Martma, T., Nam, S.-I., 2019. Discharge of meteoric water in the eastern Norwegian Sea since the last glacial period. Geophys. Res. Lett. 46 https://doi.org/10.1029/2019GL084237.

Hong, W.-L., Peszynska, M., Ruffine, L., Broseta, D., Desmedt, A., 2018. In: Geochemical Aspects. Gas Hydrates 2., vol. 2. John Wiley & Sons, Inc., pp. 219–241

Hong, W.-L., Torres, M.E., Portnov, A., Waage, M., Haley, B., Lepland, A., 2018. Variations in gas and water pulses at an Arctic seep: fluid sources and methane transport. Geophys. Res. Lett. 45 https://doi.org/10.1029/2018GL077309.

Hong, W.L., Sauer, S., Panieri, G., Ambrose, W.G., James, R.H., Plaza-Faverola, A., Schneider, A., 2016. Removal of methane through hydrological, microbial, and geochemical processes in the shallow sediments of pockmarks along eastern Vestnesa Ridge (Svalbard). Limnol. Oceanogr. 61 (S1), S324–S343.

Hovland, M., Gardner, J.V., Judd, A.G., 2002. The significance of pockmarks to understanding fluid flow processes and geohazards. Geofluids 2 (2), 127–136.

Hovland, M., Svensen, H., 2006. Submarine pingoes: indicators of shallow gas hydrates in a pockmark at Nyegga, Norwegian Sea. Mar. Geol. 228 (1–4), 15–23.

Hüpers, A., Kasemann, S.A., Kopf, A.J., Meixner, A., Toki, T., Shinjo, R., Wheat, C.G., You, C.-F., 2016. Fluid flow and water–rock interaction across the active Nankai Trough subduction zone forearc revealed by boron isotope geochemistry. Geochem. Cosmochim. Acta 193, 100–118.

James, R.H., Palmer, M.R., 2000. Marine geochemical cycles of the alkali elements and boron: the role of sediments. Geochem. Cosmochim. Acta 64 (18), 3111–3122.

Kastner, M., Elderfield, H., Martin, J.B., 1991. Fluids in convergent margins: what do we know about their composition, origin, role in diagenesis and importance for oceanic chemical fluxes? Phil. Trans. Phys. Sci. Eng. 335 (1638), 243–259.

Kim, J.-H., Torres, M.E., Hong, W.-L., Choi, J., Riedel, M., Bahk, J.J., Kim, S.-H., 2013. Pore fluid chemistry from the second gas hydrate drilling expedition in the Ulleung Basin (UBGH2): source, mechanisms and consequences of fluid freshening in the central part of the Ulleung Basin, East Sea. Mar. Petrol. Geol. 47, 99–112.

Kim, J.H., Torres, M.E., Haley, B.A., Ryu, J.S., Park, M.H., Hong, W.L., Choi, J., 2016. Marine silicate weathering in the anoxic sediment of the Ulleung Basin: evidence and consequences. Geochem. Geophys. Geosystem 17 (8), 3437–3453.

Kiss, E., 1988. Ion-exchange separation and spectrophotometric determination of boron in geological materials. Anal. Chim. Acta 211, 243–256.

Knies, J., Daszinnies, M., Plaza-Faverola, A., Chand, S., Sylta, Ø., Bünz, S., Johnson, J.E., Mattingsdal, R., Mienert, J., 2018. Modelling persistent methane seepage offshore western Svalbard since early Pleistocene. Mar. Petrol. Geol. 91, 800–811.

Knies, J., Mattingsdal, R., Fabian, K., Grøsfjeld, K., Baranwal, S., Husum, K., De Schepper, S., Vogt, C., Andersen, N., Matthiessen, J., 2014. Effect of early Pliocene uplift on late Pliocene cooling in the Arctic–Atlantic gateway. Earth Planet Sci. Lett. 387, 132–144.

Kopf, A., Deyhle, A., 2002. Back to the roots: boron geochemistry of mud volcanoes and its implications for mobilization depth and global B cycling. Chem. Geol. 192 (3–4), 195–210.

Kopf, A., Deyhle, A., Zuleger, E., 2000. Evidence for deep fluid circulation and gas hydrate dissociation using boron and boron isotopes of pore fluids in forearc sediments from Costa Rica (ODP Leg 170). Mar. Geol. 167 (1), 1–28.

Liu, X.L., Flemings, P.B., 2006. Passing gas through the hydrate stability zone at southern Hydrate Ridge, offshore Oregon. Earth Planet Sci. Lett. 241 (1–2), 211–226.

Luff, R., Greinert, J., Wallmann, K., Klaucke, I., Suess, E., 2005. Simulation of long-term feedbacks from authigenic carbonate crust formation at cold vent sites. Chem. Geol. 216 (1–2), 157–174.

Luff, R., Wallmann, K., Aloisi, G., 2004. Numerical modeling of carbonate crust formation at cold vent sites: significance for fluid and methane budgets and chemosynthetic biological communities. Earth Planet Sci. Lett. 221 (1–4), 337–353.

Maekawa, T., 2004. Experimental study on isotopic fractionation in water during gas hydrate formation. Geochem. J. 38 (2), 129–138.

Maekawa, T., Itoh, S., Sakata, S., Igari, S., Imai, N., 1995. Pressure and temperature conditions for methane hydrate dissociation in sodium-chloride solutions. Geochem. J. 29 (5), 325–329.

Marcon, Y., Ondréas, H., Sahling, H., Bohrmann, G., Olu, K., 2014. Fluid flow regimes and growth of a giant pockmark. Geology 42 (1), 63–66.

Marschall, H.R., 2018. Boron isotopes in the ocean floor realm and the mantle. In: Boron Isotopes. Springer, pp. 189–215.

Martin, J.B., Kastner, M., Henry, P., LePichon, X., Lallement, S., 1996. Chemical and isotopic evidence for sources of fluids in a mud volcano field seaward of the Barbados accretionary wedge. J. Geophys. Res. Solid Earth 101 (B9), 20325–20345.

Matsumoto, R., 2000. Methane hydrate estimates from the chloride and oxygen isotopic anomalies - examples from the Blake Ridge and Nankai trough sediments. Gas Hydrates: Challenges Future 912, 39–50.

Mattingsdal, R., Knies, J., Andreassen, K., Fabian, K., Husum, K., Grøsfjeld, K., De Schepper, S., 2014. A new 6 Myr stratigraphic framework for the Atlantic–Arctic Gateway. Quat. Sci. Rev. 92, 170–178.

Mazzini, A., Jonk, R., Duranti, D., Parnell, J., Cronin, B., Hurst, A., 2003. Fluid escape from reservoirs: implications fromcold seeps, fractures and injected sands Part i. The fluid flow system. J. Geochem. Explor. 78, 293–296.

Milkov, A.V., Dickens, G.R., Claypool, G.E., Lee, Y.J., Borowski, W.S., Torres, M.E., Xu, W.Y., Tomaru, H., Tréhu, A.M., Schultheiss, P., 2004. Co-existence of gas hydrate, free gas, and brine within the regional gas hydrate stability zone at Hydrate Ridge (Oregon margin): evidence from prolonged degassing of a pressurized core. Earth Planet Sci. Lett. 222 (3–4), 829–843.

Ondréas, H., Olu, K., Fouquet, Y., Charlou, J., Gay, A., Dennielou, B., Donval, J., Fifis, A., Nadalig, T., Cochonat, P., 2005. ROV study of a giant pockmark on the Gabon continental margin. Geo Mar. Lett. 25 (5), 281–292.

Palmer, M., Spivack, A., Edmond, J., 1987. Temperature and pH controls over isotopic fractionation during adsorption of boron on marine clay. Geochem. Cosmochim. Acta 51 (9), 2319–2323.

Pape, T., Bünz, S., Hong, W.L., Torres, M.E., Riedel, M., Panieri, G., Lepland, A., Hsu, C. W., Wintersteller, P., Wallmann, K., Schmidt, C., Yao, H., Bohrmann, G., 2020. Origin and transformation of light hydrocarbons ascending at an active pockmark on Vestnesa Ridge, Arctic Ocean. J. Geophys. Res.Solid Earth.

Peszynska, M., Hong, W.-L., Torres, M.E., Kim, J.-H., 2016. Methane hydrate formation in Ulleung Basin under conditions of variable salinity: reduced model and experiments. Transport in Porous Media, pp. 1–27.

Petersen, Carl Jörg, Bünz, Stefan, Hustoft, Steinar, Mienert, Jürgen, Klaeschen, Dirk, 2010. High-resolution P-Cable 3D seismic imaging of gas chimney structures in gas hydrated sediments of an Arctic sediment drift. Mar. Petrol. Geol. 27 (9), 1981–1994.

Phillips, F.M., Bentley, H.W., 1987. Isotopic fractionation during ion filtration: I. Theory. Geochem. Cosmochim. Acta 51 (3), 683–695.

Plaza-Faverola, A., Bünz, S., Johnson, J.E., Chand, S., Knies, J., Mienert, J., Franek, P., 2015. Role of tectonic stress in seepage evolution along the gas hydrate-charged Vestnesa Ridge, Fram Strait. Geophys. Res. Lett. 42 (3) https://doi.org/10.1002/2014GL062474.

Plaza-Faverola, A., Keiding, M., 2019. Correlation between tectonic stress regimes and methane seepage on the western Svalbard margin. Solid Earth 10, 79–94.

Plaza-Faverola, A., Vadakkepuliyambatta, S., Hong, W.-L., Mienert, J., Bünz, S., Chand, S., Greinert, J., 2017. Bottom-simulating reflector dynamics at Arctic thermogenic gas provinces: an example from Vestnesa Ridge, offshore west Svalbard. J. Geophys. Res.: Solid Earth 122 (6), 4089–4105.

Rae, J.W., Burke, A., Robinson, L., Adkins, J., Chen, T., Cole, C., Greenop, R., Li, T., Littley, E., Nita, D., 2018. CO_2 storage and release in the deep Southern Ocean on millennial to centennial timescales. Nature 562 (7728), 569–573.

Rae, J.W., Foster, G.L., Schmidt, D.N., Elliott, T., 2011. Boron isotopes and B/Ca in benthic foraminifera: proxies for the deep ocean carbonate system. Earth Planet Sci. Lett. 302 (3–4), 403–413.

Sahling, H., Bohrmann, G., Spiess, V., Bialas, J., Breitzke, M., Ivanov, M., Kasten, S., Krastel, S., Schneider, R., 2008. Pockmarks in the Northern Congo Fan area, SW Africa: complex seafloor features shaped by fluid flow. Mar. Geol. 249 (3–4), 206–225.

Seeberg-Elverfeldt, J., Schlüter, M., Feseker, T., Kölling, M., 2005. Rhizon sampling of porewaters near the sediment-water interface of aquatic systems. Limnol Oceanogr. Methods 3 (8), 361–371.

Sheppard, S., Gilg, H., 1996. Stable isotope geochemistry of clay minerals. Clay Miner. 31 (1), 1–24.

Singhroha, S., Bünz, S., Plaza-Faverola, A., Chand, S., 2020. Detection of gas hydrates in faults using azimuthal seismic velocity analysis, Vestnesa Ridge, W-Svalbard margin. J. Geophys. Res.: Solid Earth 125 (2), e2019JB017949.

Singhroha, S., Chand, S., Bünz, S., 2019. Constraints on gas hydrate distribution and morphology in Vestnesa Ridge, western svalbard margin, using multicomponent ocean-bottom seismic data. J. Geophys. Res.: Solid Earth 124 (5), 4343–4364.

Smith, A.J., Mienert, J., Bunz, S., Greinert, J., 2014. Thermogenic methane injection via bubble transport into the upper Arctic Ocean from the hydrate-charged Vestnesa Ridge, Svalbard. Geochem. Geophys. Geosystem 15 (5), 1945–1959.

Spivack, A.J., Palmer, M.R., Edmond, J.M., 1987. The sedimentary cycle of the boron isotopes. Geochem. Cosmochim. Acta 51 (7), 1939–1949.

Sultan, N., Bohrmann, G., Ruffine, L., Pape, T., Riboulot, V., Colliat, J.L., De Prunele, A., Dennielou, B., Garziglia, S., Himmler, T., 2014. Pockmark formation and evolution in deep water Nigeria: rapid hydrate growth versus slow hydrate dissolution. J. Geophys. Res.: Solid Earth 119 (4), 2679–2694.

Teichert, B.M.A., Torres, M.E., Bohrmann, G., Eisenhauer, A., 2005. Fluid sources, fluid pathways and diagenetic reactions across an accretionary prism revealed by Sr and B geochemistry. Earth Planet Sci. Lett. 239 (1–2), 106–121.

Tomaru, H., Torres, M.E., Matsumoto, R., Borowski, W.S., 2006. Effect of massive gas hydrate formation on the water isotopic fractionation of the gas hydrate system at Hydrate Ridge, Cascadia margin, offshore Oregon. Geochem. Geophys. Geosystem 7.

Torres, M.E., Kim, J.-H., Choi, J.-Y., Ryu, B.-J., Bahk, J.-J., Riedel, M., Collett, T., Hong, W.-L., Kastner, M., 2011. Occurrence of high salinity fluids associated with massive near-seafloor gas hydrate deposits. 7th International Conference on Gas Hydrates.

Torres, M.E., Wallmann, K., Trehu, A.M., Bohrmann, G., Borowski, W.S., Tomaru, H., 2004. Gas hydrate growth, methane transport, and chloride enrichment at the southern summit of Hydrate Ridge, Cascadia margin off Oregon. Earth Planet Sci. Lett. 226 (1–2), 225–241.

Tréhu, A.M., Long, P.E., Torres, M.E., Bohrmann, G., Rack, F.R., Collett, T.S., Goldberg, D.S., Milkov, A.V., Riedel, M., Schultheiss, P., Bangs, N.L., Barr, S.R., Borowski, W.S., Claypool, G.E., Delwiche, M.E., Dickens, G.R., Gracia, E., Guerin, G., Holland, M., Johnson, J.E., Lee, Y.J., Liu, C.S., Su, X., Teichert, B., Tomaru, H., Vanneste, M., Watanabe, M., Weinberger, J.L., 2004. Three-dimensional distribution of gas hydrate beneath southern Hydrate Ridge: constraints from ODP Leg 204. Earth Planet Sci. Lett. 222 (3–4), 845–862.

Ussler, W., Paull, C.K., 2001. Ion exclusion associated with marine gas hydrate deposits. In: Natural Gas Hydrates: Occurrence, Distribution, and Detection. American Geophysical Union, pp. 41–51.

Vogt, P., Gardner, J., Crane, K., Sundvor, E., Bowles, F., Cherkashev, G., 1999. Ground-truthing 11-to 12-kHz side-scan sonar imagery in the Norwegia–Greenland sea: Part

I: Pockmarks on the Vestnesa Ridge and Storegga slide margin. Geo Mar. Lett. 19 (1–2), 97–110.
Vogt, P.R., Crane, K., Sundvor, E., Max, M.D., Pfirman, S.L., 1994. Methane-generated (?) pockmarks on young, thickly sedimented oceanic crust in the Arctic: Vestnesa ridge, Fram strait. Geology 22 (3), 255–258.
Waage, Malin, Bünz, Stefan, Landrø, Martin, Plaza-Faverola, Andreia, Waghorn, Kate A., 2019. Repeatability of high-resolution 3D seismic data. Geophysics 84 (1), B75–B94.
Wallmann, K., Riedel, M., Hong, W.L., Patton, H., Hubbard, A., Pape, T., Hsu, C.W., Schmidt, C., Johnson, J.E., Torres, M.E., Andreassen, K., Berndt, C., Bohrmann, G., 2018. Gas hydrate dissociation off Svalbard induced by isostatic rebound rather than global warming. Nat. Commun. 9 (1), 83.
Yao, H., Hong, W.L., Panieri, G., Sauer, S., Torres, M.E., Lehmann, M.F., Gründger, F., Niemann, H., 2019. Fracture-controlled fluid transport supports microbial methane-oxidizing communities at Vestnesa Ridge. Biogeosciences 16 (10), 2221–2232.
Yoshimura, K., Miyazaki, Y., Ota, F., Matsuoka, S., Sakashita, H., 1998. Complexation of boric acid with the N-methyl-D-glucamine group in solution and in crosslinked polymer. J. Chem. Soc., Faraday Trans. 94 (5), 683–689.
You, C.-F., Castillo, P., Gieskes, J., Chan, L., Spivack, A., 1996. Trace element behavior in hydrothermal experiments: implications for fluid processes at shallow depths in subduction zones. Earth Planet Sci. Lett. 140 (1–4), 41–52.
You, C.-F., Chan, L., Spivack, A., Gieskes, J., 1995a. Lithium, boron, and their isotopes in sediments and pore waters of Ocean Drilling Program Site 808, Nankai Trough: implications for fluid expulsion in accretionary prisms. Geology 23 (1), 37–40.
You, C., Spivack, A., Gieskes, J., Rosenbauer, R., Bischoff, J., 1995b. Experimental study of boron geochemistry: implications for fluid processes in subduction zones. Geochem. Cosmochim. Acta 59 (12), 2435–2442.